General Disclaimer

One or more of the Following Statements may affect this Document

- This document has been reproduced from the best copy furnished by the organizational source. It is being released in the interest of making available as much information as possible.

- This document may contain data, which exceeds the sheet parameters. It was furnished in this condition by the organizational source and is the best copy available.

- This document may contain tone-on-tone or color graphs, charts and/or pictures, which have been reproduced in black and white.

- This document is paginated as submitted by the original source.

- Portions of this document are not fully legible due to the historical nature of some of the material. However, it is the best reproduction available from the original submission.

Spectral Line Profiles for a Planetary Corona

Joseph W. Chamberlain

Department of Space Physics and Astronomy

Rice University, Houston, Texas 77001

Abstract

The Lyman and Balmer emission of a planetary corona depend on the exospheric temperature, the integrated column density of solar-illuminated hydrogen, and the region of phase space occupied by particles. Measurements of the intensity alone are incapable of defining the exosphere unambiguously. Line profiles, with high spectral resolution, can show whether a non-thermal component of the escaping hydrogen is present and can indicate at what altitude satellite orbits of hydrogen atoms are depleted. It is necessary, however, to plan the observations carefully if they are to be fitted usefully to a model.

I. Introduction

Two matters of substance complicate the interpretation of direct optical observations of a planetary corona: the component temperatures and the degree to which satellite orbits are present are generally unknown.

The temperature problem evidently exists for the earth's corona, even though independent scale-height measures from satellite drag are

(NASA-CR-143320) SPECTRAL LINE PROFILES FOR A PLANETARY CORONA (Rice Univ.) 16 p HC $3.25 CSCL 03B

N75-30979

Unclas
G3/91 33030

available. The difficulty is that intensity observations of Lyα require a higher escaping flux of hydrogen than can be accounted for by thermal escape of H atoms (Hunten, 1973 ; Hunten and Strobel, 1974; Liu and Donahue, 1974; Bertaux, 1975; Tinsley, et al., 1975; Thomas and Anderson, 1975). [More precisely, observed variations of the temperature and intensity of Lyα imply large time variations in the thermal evaporation of H atoms. But the total loss of hydrogen must be constant, because the upward flow is limited by eddy diffusion much lower in the atmosphere. Hence additional escape that compensates for the fluctuations in thermal evaporation is implied.] It becomes necessary to invoke an additional mechanism, either charge exchange of cold H with hot H^+ (Cole, 1966; Tinsley, 1973; Tinsley et al., 1975) or a chemical mechanism that releases H atoms with high velocity. To the extent that the non-thermal mechanism is important, the ordinary exospheric scale height is unhelpful.

The temperature problem may also exist for Venus (McElroy, 1969; Kumar and Hunten, 1974), where Mariner IV observations suggested a superposition of two intermingled coronae with distinct temperatures.

The problem of satellite orbits is equally unsettling, as we have neither observation nor theory to indicate the extent that such orbits are populated. My earlier paper (Chamberlain, 1963, Sec. 6b) suggested an equilibrium might be established by the creation of satellites through collisions and their destructic through both collisions and photoionization. More likely, radiation pressure, which can distort circular orbits into elliptical ones and lower their perigees (Slowey, 1969; Thomas and Bohlin, 1972; Bertaux and Blamont, 1973), is the dominant destruction mechanism. If so, variations of solar Lyα could alter the effective base level of satellite orbits, so that no single distribution of orbits would be universally appropriate.

Therefore, it seems likely that the few data we have need to be supplemented. The measurement of line profiles with high spectral resolution might clarify matters. The basic theory for profiles was developed earlier (Chamberlain, 1963, Sec. 7) but no numerical calcula-

tions were made. Here I wish to indicate the kind of profile that can be expected for the simplest possible situation: a single temperature, radially outward observations, and a well-defined "satellite critical level" (the maximum perigee for satellite orbits). The theory can be generalized for a two-component gas, but the examples given here should suffice to outline the problem. The only measurements available to date (Atreya, Hays, and Nagy, 1975) were not interpreted with allowance for the vacant orbits, and the long time-integration of their observations would in any case make it difficult to construct an appropriate coronal model. In principle, the spectrum could be computed for an arbitrary direction of observation, but the problem is enormously simplified if the observations are made toward the zenith.

II. Profile Theory: A Summary

The radial Doppler profile is

$$4\pi I(v_r, \lambda_1) = g(\mathrm{Ly}\alpha)\,\frac{N_c\, r_c \lambda_c\, e^{-\lambda_c}\, e^{-\xi^2}}{U\pi^{1/2}}\, S(\xi, \lambda_1). \qquad (1)$$

Here I is the photon intensity for a Doppler displacement v_r, when the shadow height intersects the line of sight at distance r_1 from the planet's center. The dimensionless units used in the theory are

$$\lambda = \frac{GMM}{kT_c r}\,,\quad \xi = \frac{v_r}{U}\,,\quad \nu = \frac{v_\perp^2}{U^2}\,, \qquad (2)$$

where $U = 2kT_c/M$, M is the mass of the planet, M the mass of the hydrogen atom, and N_c and T_c the H density and the Maxwellian temperature, respectively, at the critical level, r_c. The g(Lyα)-factor is the

number of solar photons scattered in all directions per second per H atom (Chamberlain 1961, p 425). We neglect multiple scattering, assuming an optically thin corona. An added refinement would include the anisotropy of resonance scattering in the g-factor (Brandt and Chamberlain 1959).

The factor $S(\xi,\lambda_1)$ in equation (1) is the "radial spectrum function",

$$S(\xi,\ \lambda_1) = \int_0^{\lambda_1}\int_{\nu} \frac{e^{\lambda}\ e^{-\nu}}{\lambda^2}\ d\nu d\lambda\ . \qquad (3)$$

If all the Maxwellian orbits were filled (with all velocities and all directions), S would be independent of ξ and the profile would be gaussian. In this case, however, S would also be infinite. In the realistic case, wherein dynamical constraints are placed on allowed orbits, the integrated density above r_1,

$$N(\lambda_1) = \frac{4\pi}{g}\int I(v_r,\ \lambda_1)dv_r\ , \qquad (4)$$

is finite. Tables exist (Chamberlain 1963, Tables 3 and 4) for computing $N(\lambda_1)$ for various assumed parameters.

To evaluate the spectrum function (3), it is convenient to divide particle orbits into three categories: ballistic (gravitationally bound and intersecting r_c), satellite (bound but lying wholly above r_c), and escaping. The ballistic plus satellite orbits are collectively called "captive", and their integral is rather simple:

$$S_{cap}(\xi,\ \lambda_1) = \int_{\xi^2}^{\lambda_1} \frac{e^{\lambda}}{\lambda^2}\ (1 - e^{-\nu_2})d\lambda\ , \qquad (5)$$

where

$$\nu_2(\xi) = \lambda - \xi^2 \quad . \tag{6}$$

For S_{cap} the ν integration involves only the condition of negative energy; it represents the totality of oribts above r, with velocity v_r.

For ballistic orbits we have the added condition that the orbits intersect r_c. This integral is more complicated; for reasons that will become clear, we carry the functional notation λ_c explicity:

$$S_{bal}(\lambda_c; \xi, \lambda_1) = \int_{\xi 2}^{\lambda_{2-}} \frac{e\lambda}{\lambda^2}(1 - e^{-\nu_2})d\lambda$$

$$+\int_{\lambda_{2-}}^{\lambda_{2+}} \frac{e\lambda}{\lambda^2}(1 - e^{-\nu_1})d\lambda + \int_{\lambda_{2+}}^{\lambda_1} \frac{e\lambda}{\lambda^2}(1 - e^{-\nu_2})d\lambda \ , \tag{7}$$

where

$$\nu_1(\xi) = \frac{\lambda^2}{(\lambda_c^2 - \lambda^2)}(\lambda_c - \lambda + \xi^2) \tag{8}$$

and

$$\lambda 2_{\pm}(\xi, \lambda_c) = \frac{\lambda_c}{2}\left[1 \pm \left(1 - \frac{4\xi^2}{\lambda_c}\right)^{1/2}\right] . \tag{9}$$

The totality of all possible satellite oribts is then

$$S_{sat}(\lambda_c; \xi, \lambda_1) = S_{cap}(\xi, \lambda_1) - S_{bal}(\lambda_c; \xi, \lambda_1), \tag{10}$$

which yields

$$S_{sat}(\lambda_c; \xi, \lambda_1) = \int_{\lambda_{2-}}^{\lambda_{2+}} \frac{e^{\lambda}}{\lambda^2} (e^{-\nu_1} - e^{-\nu_2}) d\lambda \ . \quad (11)$$

It must be emphasized that, although λ_1 does not appear explicitly on the right side, when λ_1 is less than λ_{2+} (or even λ_{2-}), the λ_1 limit prevails.

The escaping component is analogous to the ballistic:

$$S_{esc}(\lambda_c; \xi, \lambda_1) = \int_0^{\xi_2} \frac{e^{\lambda}}{\lambda^2} (1 - e^{-\nu_1}) d\lambda$$

$$+ \int_{\xi^2}^{\lambda_{2-}} \frac{e^{\lambda}}{\lambda^2} (e^{-\nu_2} - e^{-\nu_1}) d\lambda \quad + \int_{\lambda_{2+}}^{\lambda_1} \frac{e^{\lambda}}{\lambda^2} (e^{-\nu_2} - e^{-\nu_1}) d\lambda \quad (12)$$

for $\xi > 0$ and

$$S_{esc}(\lambda_c; \xi, \lambda_1) = 0 \quad (13)$$

for $\xi \leq 0$. Note that there is a region $\lambda_{2-} < \lambda < \lambda_{2+}$ that is empty of escaping particles. However, when $\xi > \lambda_c^{1/2}/2$, both λ_{2-} and λ_{2+} are imaginary and the separate integrals involving these limits in equations (7) and (12) merge into a single one and $S_{sat} = 0$.

In practice all possible satellite orbits are not expected to be present. A simple artifice for specifying those present is to define a second or "satellite" critical level r_c^*, above r_c. We will assume that any captive particle with a perigee below r_c^* is present; then the satellite and ballistic particles are given by $S_{bal}(\lambda_c^*; \xi, \lambda_1)$, and λ_c is changed to λ_c^* in equations (7) through (11).

We now distinguish two cases. First, when the shadow height, r_1, is above r_c^*, we have simply

$$S(\xi, \lambda_1 < \lambda_c^*) = S_{bal}(\lambda_c^*; \xi, \lambda_1) + S_{esc}(\lambda_c; \xi, \lambda_1). \quad (14)$$

When the shadow height is below r_c^*, we integrate all bound orbits from r_1 up to r_c^* but include above r_c^* only those orbits intersecting r_c^*. Thus we write

$$S(\xi, \lambda_1 > \lambda_c^*) = S_{cap}(\xi, \lambda_1) - S_{sat}(\lambda_c^*; \xi, \lambda_c^*)$$

$$+ S_{esc}(\lambda_c; \xi, \lambda_1). \quad (15)$$

Equation (14) may be put in the same form as equation (15) by substituting $S_{bal}(\lambda_c^*; \xi, \lambda_1)$ from equation (10):

$$S(\xi, \lambda_1 < \lambda_c^*) = S_{cap}(\xi, \lambda_1) - S_{sat}(\lambda_c^*; \xi, \lambda_1)$$

$$+ S_{esc}(\lambda_c; \xi, \lambda_1). \quad (16)$$

Equations (15) and (16) are convenient for computations when λ_c^* is unknown and spectrum functions are to be calculated with varying λ_c^* to obtain a best fit with observations. First $S(\xi, \lambda_1)$ is computed for $\lambda_c^* = 0$, then S_{sat} may be substracted for any specified λ_c^*.

III. Sample Profiles

Throughout the examples shown here, we chose $\lambda_c = 7.5$, corresponding to r_c being 500 km above the surface of earth and $T_c = 938\,^{\circ}K$ for H. The curves in Figure 1 show a range of shadow heights and satellite critical levels, r_c^*.

The curves illustrate our contention that good profiles could help distinguish the best r_c^* as well as the exospheric temperature(s). For the full satellite distribution ($\lambda_c^* = 0$), there is a drastic cut-off of the profile's wings (compared with a gaussian profile) because of the absence of orbiting particles exceeding the escape velocity. When the satellites are removed altogether ($\lambda_c^* = 7.5$), the line center is depleted the most, which relatively enhances the wings. The asymmetry of the two sides of the profile becomes enhanced, as escaping particles (or their absence) become relatively more important.

Figures 2 and 3 illustrate the two-dimensional phase space that contributes to the profiles and may help provide some rationale for why the profiles in Figure 1 have such peculiar shapes. The shaded areas are forbidden regions -- where particles are excluded by the dynamical restrictions. These regions are defined by

$$\xi^2 < (\lambda_c^* - \lambda)\left[\frac{\nu_c^* (\lambda_c^* + \lambda)}{\lambda_c^{*2}} - 1\right] \qquad (17)$$

where $\nu_c^* = \nu_c \lambda_c^{*2}/\lambda_c^2$, and

$$\xi < -\left(\lambda - \frac{\lambda^2 \nu_c}{\lambda_c^2}\right)^{1/2} . \qquad (18)$$

The first restriction requires all orbits to intersect the sphere of radius r_c^*, whereas the second excludes particles of positive energy from the downward-directed hemisphere.

Acknowledgment

This research was supported in part by the National Aeronautics and Space Administration through grant NSG-7043 and by the Atmospheric Sciences Section, National Science Foundation, through grant GA-41788.

Legends

Fig. 1 - Spectrum functions for various shadow heights, r_1, and satellite critical levels, r_c, for zenith observations from below r_1. In all cases the base of the exosphere is specified by $\lambda_c = 7.5$ (e.g., appropriate for 500 km altitude on earth, with H atoms at 938 °K). For $\lambda_c^* = 7.5$ all satellite orbits are depleted; for $\lambda_c^* = 0$, all possible satellite orbits for negative total energy are filled, so that particles at any height are isotropic for all velocities less than $\lambda^{1/2}$. The curves, when multiplied by $\exp(-\xi^2)$, give the Doppler line profiles.

Fig. 2 - Phase-space diagram showing (by cross-hatched areas) regions in which orbits are forbidden for $\lambda_c^* = \lambda_c = 7.5$. In this case no satellite orbits are filled; when present (i.e., when $\lambda_c^* = 0$) the central forbidden regions are absent. The shaded areas on the left of each diagram are downward directed orbits with velocities exceeding the local escape velocity. When the transverse kinetic energy at the critical level, v_c, exceeds the gravitational energy, λ_c, the two forbidden regions overlap. On this diagram a particle orbit close to a forbidden region is a curve roughly parallel to the boundary of the region.

Fig. 3 - Forbidden regions in dimensionless phase space for identical transverse kinetic energies ($\nu_c = 5.0$), $\lambda_c = 7.5$, and different satellite critical levels, λ_c^*. See legend to Figure 2. For $\lambda_c^* = 7.5$ the diagram fits into the sequence of Figure 2. For $\lambda_c^* \leq \lambda_c^2/2\nu_c = 5.625$, no satellite orbits are forbidden. In intermediate cases the forbidden region of satellite orbits lies at $\lambda < \lambda_c^*$ and is fixed by the dynamical condition that allowed orbits in this region must intersect λ_c^*.

References

Atreya, S. K., P. B. Hays, and A. J. Nagy, Doppler profile measurements of the geocoronal hydrogen balmer alpha line, J. Geophys. Res., 80, 635, 1975.

Bertaux, J. L., Observed variations of the exospheric hydrogen density with the exospheric temperature, J. Geophys. Res., 80, 639, 1975.

Bertaux, J. L. and J. E. Blamont, Interpretation of Ogo 5 Lyman alpha measurements in the upper geocorona, J. Geophys. Res., 78, 80, 1973.

Brandt, J. C. and J. W. Chamberlain, Interplanetary gas I. Hydrogen radiation in the night sky, Ap. J., 130, 670, 1959.

Chamberlain, J. W., Planetary coronae and atmospheric evaporation, Planet. Space Sci., 11, 901, 1963.

Chamberlain, J. W., Physics of the Aurora and Airglow, Acdaemic Press, New York, 1961.

Cole, K. D., Theory of some quiet magnetospheric phenomena related to the geomagnetic tail, Nature, 211, 1385, 1966.

Hunten, D. M., The escape of light gases from planetary atmospheres, J. Atmosph. Sci., 30, 1481, 1973.

Hunten, D. M. and D. F. Strobel, Production and escape of terrestrial hydrogen, J. Atmosph. Sci., 31, 305, 1974.

Kumar, S. and D. M. Hunten, Venus: An ionospheric model with an exospheric temperature of 350°K, J. Geophys. Res., 79, 2529, 1974.

Lui, S. C. and T. M. Donahue, Realistic model of hydrogen constituents in the lower atmosphere and escape flux from the upper atmosphere, J. Atmosph. Sci., 31, 2238, 1974.

McElroy, M. B., Structure of the Venus and Mars atmospheres, J. Geophys. Res., 74, 29, 1969.

Slowey, J. W., The effect of solar-radiation pressure on determination of the semimajor axis in satellite-orbit computation, Space Research, IX, 76, 1969.

Thomas, G. E. and D. E. Anderson, Jr., Global atomic hydrogen density from Lα airglow measurements from the OGO-6 satellite, Planet. Space Sci., in press, 1975.

Thomas, G. E. and R. C. Bohlin, Lyman-alpha measurements of neutral hydrogen in the outer geocorona and in interplanetary space, J. Geophys. Res., 77, 2752, 1972.

Tinsley, B. A., The diurnal variation of atomic hydrogen, Planet. Space Sci., 21, 686, 1973.

Tinsley, B. A., R. R. Hodges, Jr., and D. F. Strobel, Diurnal variations of atomic hydrogen: observations and calculations, J. Geophys. Res., 80, 626, 1975.

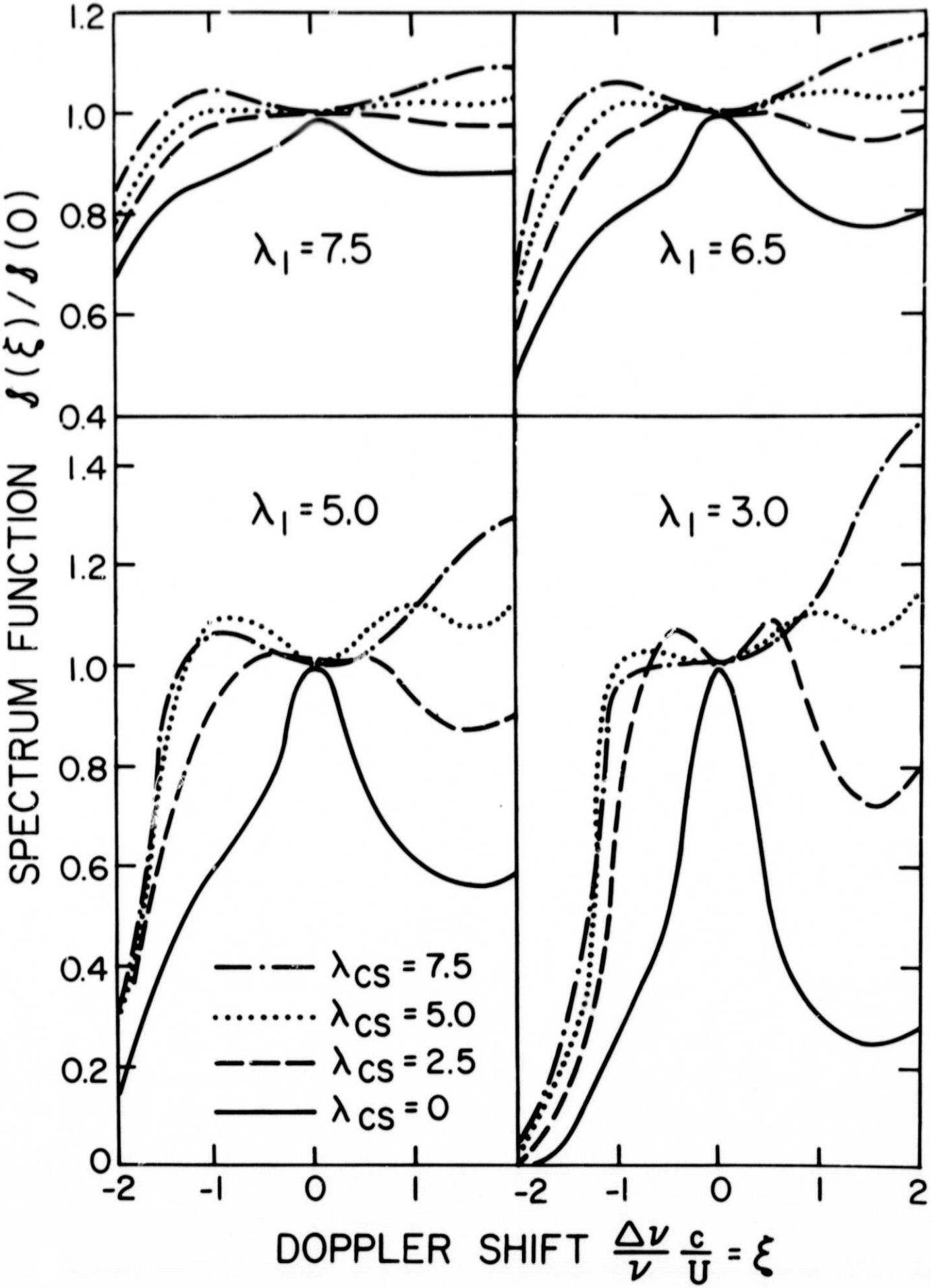
SPECTRUM FUNCTION $\mathcal{S}(\xi)/\mathcal{S}(0)$
DOPPLER SHIFT $\frac{\Delta\nu}{\nu}\frac{c}{U} = \xi$
$\lambda_1 = 7.5$
$\lambda_1 = 6.5$
$\lambda_1 = 5.0$
$\lambda_1 = 3.0$
$\lambda_{CS} = 7.5$
$\lambda_{CS} = 5.0$
$\lambda_{CS} = 2.5$
$\lambda_{CS} = 0$
0
0.2
0.4
0.6
0.8
1.0
1.2
1.4
-2
-1
0
1
2

ν_c=6.0
λ^*_c=7.5
ν_c=2.0
λ^*_c=7.5
λ^*_c=7.5
ν_c=8.0
λ^*_c=7.5
ν_c=4.0
λ
ξ

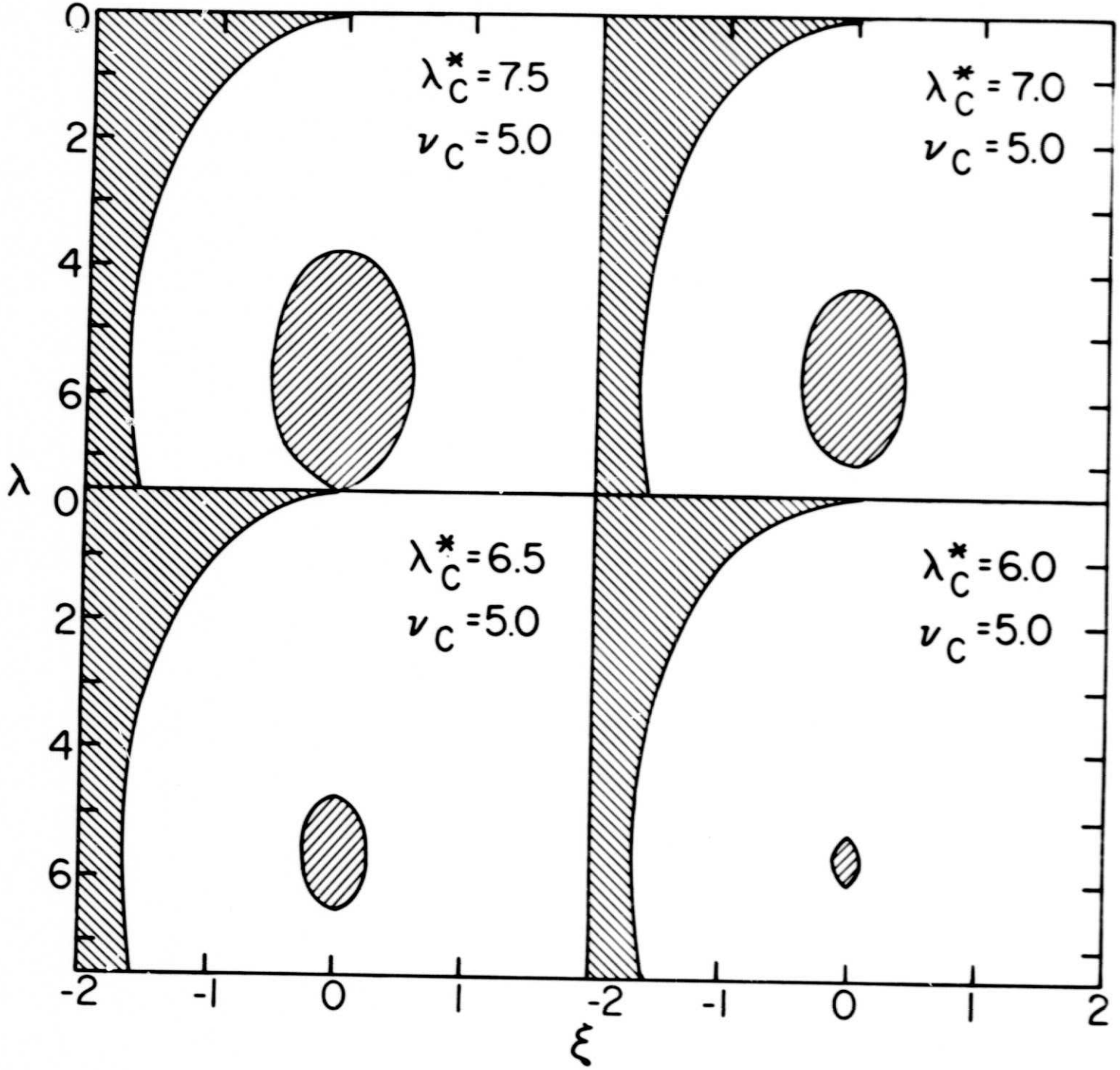
$\lambda_c^* = 7.5$
$\nu_c = 5.0$
$\lambda_c^* = 7.0$
$\nu_c = 5.0$
$\lambda_c^* = 6.5$
$\nu_c = 5.0$
$\lambda_c^* = 6.0$
$\nu_c = 5.0$
λ
ξ
0
2
4
6
-2
-1
0
1
2